



## OPEN Peroxiredoxin 6 maintains mitochondrial homeostasis and promotes tumor progression through ROS/JNK/p38 MAPK signaling pathway in multiple myeloma

Dandan Gao<sup>1</sup>, Yang Lv<sup>1</sup>, Fei Hong<sup>1</sup>, Dong Wu<sup>1</sup>, Ting Wang<sup>1</sup>, Gongzhizi Gao<sup>1</sup>, Zujie Lin<sup>1</sup>, Ruoyu Yang<sup>1</sup>, Jinsong Hu<sup>2</sup>, Aili He<sup>1,3,4,5</sup>✉ & Pengyu Zhang<sup>1</sup>✉

Peroxiredoxin 6 (PRDX6) is one of the Peroxiredoxin family members with only 1-Cys, using glutathione as the electron donor to reduce peroxides in cells. PRDX6 has been frequently studied and its expression was associated with poor prognosis in many tumors. However, the expression of PRDX6 in multiple myeloma (MM) and its relevance with MM remain unclear. In our study, we found that PRDX6 was overexpressed in MM patients. Its high expression was inversely correlated with prognosis but positively correlated with the levels of  $\beta$ 2-microglobulin (B2M), lactate dehydrogenase (LDH), and International Staging System (ISS) stage of MM patients. Further, the deficiency of PRDX6 promoted MM cell lines (RPMI 8226, MM.1S, and U266) apoptosis significantly. Mechanically, PRDX6 serves as an anti-oxidative enzyme, and its deficiency led to over-accumulation of reactive oxygen species (ROS), resulting in oxidative stress, following the activation of MAPK signaling pathway, which manifested as phosphorylation of JNK and p38. Then, the expression of BAX and Bcl2 was imbalance, and the cascade cleavage of PARP and caspase 3 was increased, ultimately triggering cell apoptosis. In addition, oxidative stress decreased mitochondrial membrane potential (MMP), reduced gene expression levels of oxidative phosphorylation (OXPHOS), and increased in the density of mitochondrial crumpling, leading to mitochondrial structural abnormalities and dysfunction. Furthermore, PRDX6 deficiency combined with bortezomib induced a robust anti-tumor effect in MM cell lines. Finally, in vivo experiments also showed that the deficiency of PRDX6 inhibited tumor growth of tumor-bearing mice. Collectively, PRDX6 protects MM cells from oxidative damage and maintains mitochondrial homeostasis. And targeting PRDX6 is an attractive strategy to enhance the anti-tumor effect of bortezomib in MM.

**Keywords** Multiple myeloma, Apoptosis, Reactive oxygen species, Mitochondrial homeostasis, Bortezomib

The second most prevalent hematologic malignancy, multiple myeloma (MM), is characterized by uncontrolled expansion of aberrant plasma cells in the bone marrow, which produces an excessive amount of monoclonal immunoglobulin, ultimately leading to hypercalcemia, renal impairment, anemia, or pathologic fracture. Although many novel regimens have been developed to improve MM patients' outcomes over the past decades, the disease is still incurable<sup>1</sup>. Proteasome inhibitors (PIs), particularly bortezomib (BTZ), are one of those that significantly improve the overall survival (OS) of MM patients<sup>2</sup>. Nevertheless, a lot of patients relapsed after

<sup>1</sup>Department of Hematology, The Second Affiliated Hospital of Xi'an Jiaotong University, No. 157, West 5th Road, Xi'an, Shaanxi, China. <sup>2</sup>Department of Cell Biology and Genetics, Xi'an Jiaotong University Health Science Center, Xi'an, Shaanxi, China. <sup>3</sup>Xi'an Key Laboratory of Hematological Diseases, Xi'an, China. <sup>4</sup>Department of Tumor and Immunology in Precision Medical Institute, Xi'an Jiaotong University, Xi'an, China. <sup>5</sup>National-Local Joint Engineering Research Center of Biodiagnostics & Biotherapy, The Second Affiliated Hospital of Xi'an Jiaotong University, Xi'an, Shaanxi, China. ✉email: heaili@xjtu.edu.cn; zhangpengyu2004@126.com

receiving initial treatment and developed drug resistance<sup>3</sup>. Thus, it is essential to elucidate the molecular basis of MM pathogenesis and explore effective strategies to enhance the anti-tumor effect of bortezomib in MM.

Peroxiredoxins (PRDXs), the highly conserved family, are sought to be antioxidant enzymes because they can reduce all kinds of peroxide, including hydrogen or lipid peroxides, protecting cells from oxidative damage. There are currently six members of this family, which were divided into two groups: 2-Cys (cysteine) PRDXs and 1-Cys PRDX<sup>4</sup>. The 2-Cys PRDXs, including PRDX1-PRDX5, utilize thioredoxin as the physiological reductant<sup>5</sup>. The sole 1-Cys PRDX (PRDX6) uses glutathione rather than thioredoxin as the electron donor<sup>6</sup>. In addition, PRDX6 is a multifunctional enzyme, which exhibits calcium-independent phospholipase (iPLA2) activity, lysophosphatidylcholine acyl transferase (LPCAT) activity, and glutathione peroxidase (Gpx) activity<sup>7</sup>. Recent research demonstrated that the expression of PRDX6 is overexpressed in a variety of solid tumors, including lung, ovarian, tongue, and breast cancer<sup>8–11</sup>. Furthermore, some studies revealed that overexpression of PRDX6 in tumors reduces their sensitivity to radiation and chemotherapy, while inhibiting PRDX6 could make tumor cells more sensitive to chemotherapy<sup>10,12,13</sup>. Although the well-established cytoprotective potential of PRDX6 in solid tumors, its role in MM and the underlying molecular mechanism are unknown.

In this study, we characterized the role of PRDX6 in MM in vitro and in vivo, and illustrated the potential mechanism. We found that PRDX6 was overexpressed in MM patients and its high expression was inversely correlated with OS, but associated with higher lactate dehydrogenase (LDH) and  $\beta$ 2-microglobulin (B2M) levels. Deficiency of PRDX6 significantly promoted apoptosis in MM cell lines. Importantly, our research demonstrated that downregulation of PRDX6 promoted bortezomib induced apoptosis, leading to a synergistic anti-tumor effect in MM. Mechanically, PRDX6 deficiency increased apoptosis rate primarily by causing the overaccumulation of reactive oxygen species (ROS), which was then followed by a reduction in mitochondrial membrane potential (MMP) and mitochondrial dysfunction. Finally, we demonstrated that the deficiency of PRDX6 significantly inhibited tumor growth in a tumor-bearing mouse model. In conclusion, our data indicated that PRDX6 is crucial in MM progression, and targeting PRDX6 may be a promising strategy to enhance the anti-tumor effect of bortezomib in MM.

## Results

### PRDX6 is overexpressed in MM and correlated with poor prognosis

Based on publicly available microarray data from the GEO database, we found the expression of PRDX6 was remarkably overexpressed in MM patients compared with healthy donors (HD) in GSE6477 ( $n=162$ ), GSE47552 ( $n=99$ ) and GSE13591 ( $n=158$ ) (Fig. 1A–C) (Supplementary Fig. 1A–C). To test the association between its expression and overall survival (OS) of MM patients, we evaluated the survival curves in GSE24080 ( $n=559$ ) and GSE57317 ( $n=55$ ). The curves revealed that PRDX6 expression was negatively correlated with the OS of MM patients (Fig. 1D–E) (Supplementary Fig. 1D–I). Subsequently, the relationship between PRDX6 expression and patients' clinical characteristics was assessed in GSE24080. The results showed that PRDX6 expression was positively correlated with the levels of  $\beta$ 2-microglobulin (B2M), lactate dehydrogenase (LDH), and ISS stage of MM patients (Table 1). Additionally, the result also indicated that complete remission (CR) rate in the low PRDX6 expression group was higher than high PRDX6 expression group ( $p<0.05$ ) (Supplementary Table 3). Collectively, these findings indicated that the patients in the PRDX6 high-expression group had poor prognosis and clinical characteristics, suggesting that PRDX6 may have a significant role in the onset of MM. Furthermore, we performed receiver operating characteristics (ROC) curves to assess the diagnostic value of PRDX6 in GSE6477. Notably, the area under the curve (AUC) was 0.8259 ( $P<0.0001$ , 95%CI: 0.7321–0.9197) for HD and newly diagnosed multiple myeloma (NDMM) (Fig. 1F). These figures demonstrated that PRDX6 might function as a biomarker to discriminate HD from different stages of plasma cell neoplasm, except for monoclonal gammopathy of undetermined significance (MGUS).

In the meanwhile, we used qRT-PCR and western blotting to assess the mRNA and protein levels of PRDX6 in BM aspirates from clinical MM patients and different MM cell lines. The results showed that PRDX6 mRNA expression was significantly elevated in MM patients (Fig. 1G,H) and MM cell lines (Fig. 1I) compared with healthy donors and HS5 (human immortalized bone marrow stromal cell line). In addition, the protein level of PRDX6 was also markedly upregulated in NDMM and MM cell lines (Fig. 1J) (Supplementary Fig. 2). Taken together, these findings suggested that PRDX6 may play an important role in MM development and progression.

### Deficiency of PRDX6 promotes apoptosis and inhibits proliferation in vitro

To determine the function of PRDX6 in MM, we conducted the RNA interference strategy to knock down PRDX6 expression in MM cell lines (RPMI 8226, MM.1S, and U266). With specific PRDX6-siRNA, the PRDX6 expression was decreased by 50–80% in different MM cell lines, as shown by western blotting and qRT-PCR (Fig. 2A,B). Then we performed the CCK-8 assay and found that the deficiency of PRDX6 remarkably decreased cell viability of MM cells (Fig. 2C). Further, we used Annexin V/7-AAD staining to examine whether cell apoptosis could be affected by the deficiency of PRDX6. As a result, after transfection of MM cells with PRDX6-siRNA, MM cells displayed a significant increase in apoptosis rate (Fig. 2D). Moreover, EdU assay was performed to detect cell proliferation, and we noted that the deficiency of PRDX6 had a small but substantial impact on reducing cell proliferation (Fig. 2E). Next, cell cycle was measured by PI staining, the results showed that PRDX6 deficiency led to cell cycle arrest at the G2/M phase (Fig. 2F). These evidence indicated that PRDX6 may affect the apoptosis, proliferation and cell cycle, which in turn affect the survival and progression of MM.

### PRDX6 protects MM cells from oxidative stress and maintains mitochondrial homeostasis

Given the antioxidant effect of PRDX6, we measured the intracellular ROS level after PRDX6 deficiency using 2',7'-dichlorofluorescein diacetate (DCFH-DA). We noted that compared with the control group, deficiency of PRDX6 significantly increased ROS level by approximately more than 1.5 times in both U266 and MM.1S

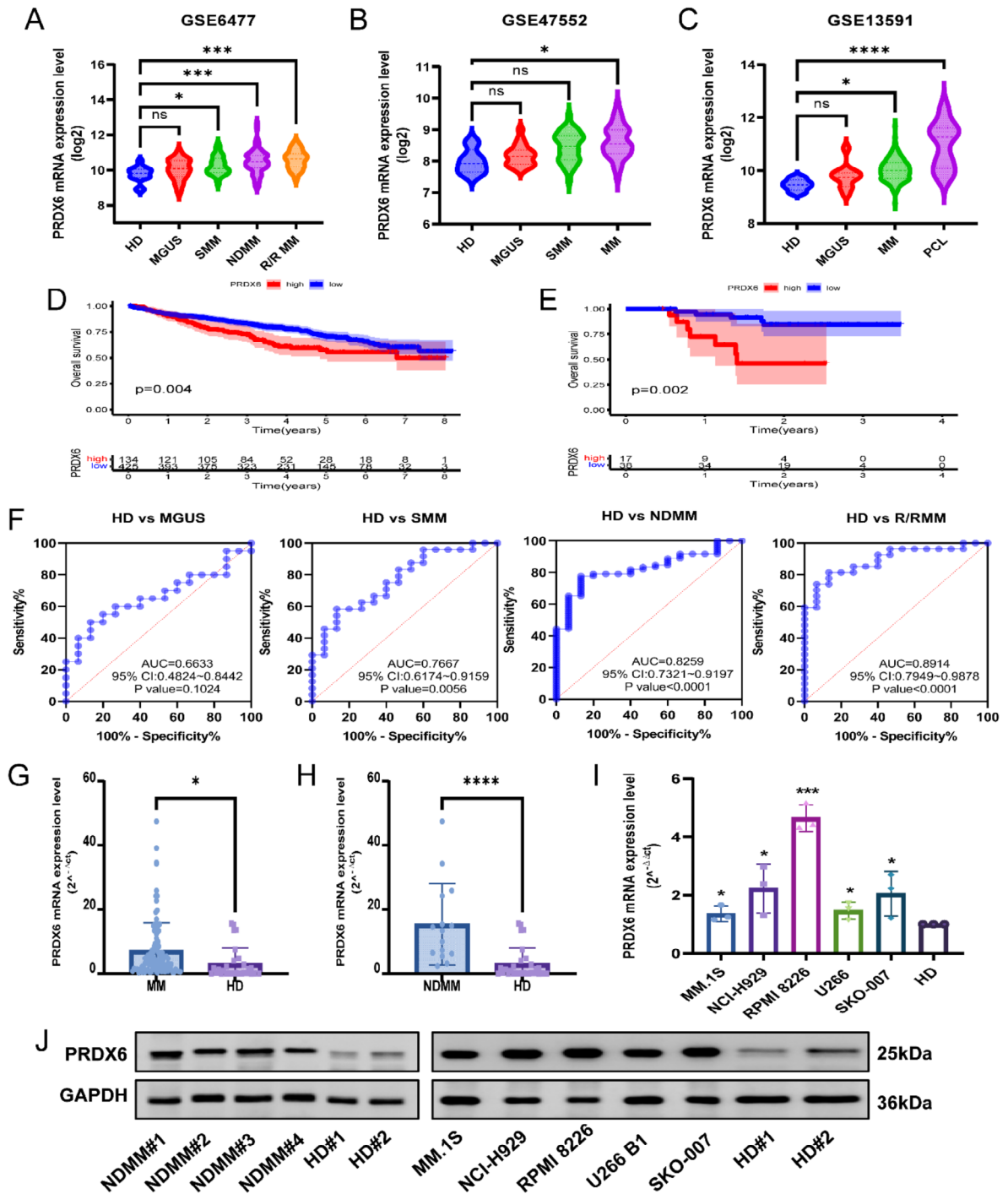


**Fig. 1.** PRDX6 is overexpressed in MM and correlated with poor prognosis of MM patients. (A–C) Analysis of PRDX6 mRNA expression in BM of patients with different stages of plasma cell neoplasm or healthy donors in GSE6477 ( $n = 162$ ) (HD, healthy donors,  $n = 15$ ; MGUS, monoclonal gammopathy of undetermined significance,  $n = 22$ ; SMM, smoldering multiple myeloma,  $n = 24$ ; NDMM, newly diagnosed multiple myeloma,  $n = 73$ ; R/RMM, relapsed or refractory multiple myeloma,  $n = 28$ ), GSE47552 ( $n = 99$ ) (HD,  $n = 5$ ; MGUS,  $n = 20$ ; SMM,  $n = 33$ ; MM,  $n = 741$ ), GSE13591 ( $n = 158$ ) (HD,  $n = 5$ ; MGUS,  $n = 11$ ; MM,  $n = 133$ ; PCL,  $n = 9$ ). (D,E) Kaplan-Meier (KM) survival analysis of PRDX6 in different stages of plasma cell neoplasm in GSE24080 ( $n = 559$ ) (D) and GSE57317 ( $n = 55$ ) (E). (F) ROC curves of PRDX6 in different stages of plasma cell neoplasm in GSE6477. The AUC and p-value were calculated. (G) Analysis of PRDX6 mRNA expression in MM patients ( $n = 84$ ) and HD ( $n = 29$ ) by qRT-PCR. (H) Analysis of PRDX6 mRNA expression in NDMM patients ( $n = 15$ ) and HD ( $n = 29$ ) by qRT-PCR. (I) Analysis of PRDX6 mRNA expression in different MM cell lines and HD by qRT-PCR. (J) Analysis of PRDX6 protein expression in NDMM patients ( $n = 4$ ) and MM cell lines compared with HD ( $n = 2$ ) by Western blotting. The data are the mean  $\pm$  SD. \* $p < 0.05$ , \*\*\* $p < 0.001$ , \*\*\*\* $p < 0.0001$ , ns: no significance.

	Low PRDX6 expression (n = 280)	High PRDX6 expression (n = 279)	t or $\chi^2$ /p-value
Gender			1.006/0.316
Male	163/280 (58.21%)	174/279 (62.37%)	
Female	117/280 (41.79%)	105/279 (37.63%)	
Age (year)	56.72 $\pm$ 9.89	57.64 $\pm$ 9.01	-1.145/0.253
Immunoglobulin subtypes			4.008/0.405
IgA	77/274 (28.10%)	56/265 (21.13%)	
IgG	154/274 (56.21%)	159/265 (60.00%)	
IgD	1/274 (0.37%)	2/265 (0.76%)	
Light Chain	39/274 (14.23%)	45/265 (16.98%)	
Nonsecretory	3/274 (1.09%)	3/265 (1.13%)	
B2M			4.012/0.045
< 3.5 mg/L	172	148	
$\geq$ 3.5 mg/L	108	131	
CRP			0.972/0.324
< 6 mg/L	171	159	
$\geq$ 6 mg/L	107	118	
CREAT ( $\mu$ mol/L)	1.24 $\pm$ 1.06	1.41 $\pm$ 1.45	-1.611/0.108
ALB			0.148/0.700
< 3.5 g/L	37	40	
$\geq$ 3.5 g/L	243	239	
HGB (g/dL)	11.38 $\pm$ 1.81	11.13 $\pm$ 1.81	1.605/0.109
LDH			7.192/0.007
< 150 U/L	142	110	
$\geq$ 150 U/L	138	169	
BMPC (%)	45.51 $\pm$ 26.12	47.27 $\pm$ 26.45	-0.780/0.436
Cyto Abn			3.504/0.061
Yes	187/280 (66.79%)	165/279 (59.14%)	
No	93/280 (33.21%)	114/279 (50.86%)	
ISS stage			4.052/0.044
I + II	167/268 (62.31%)	144/268 (53.73%)	
III	101/268 (37.69%)	124/268 (46.27%)	
Recurrence			0.001/0.978
No	196/280 (70.00%)	195/279 (69.89%)	
Yes	84/280 (30.00%)	84/279 (30.11%)	

**Table 1.** Clinical characteristics of MM patients according to the expression of PRDX6 in GSE24080 datasets ( $n = 559$ ). MM multiple myeloma, PRDX6 peroxiredoxin 6, B2M  $\beta$ 2-microglobulin, CRP C-reactive protein, CREAT creatinine, ALB albumin, HGB hemoglobin, LDH lactate dehydrogenase, BMPC bone marrow plasma cells, Cyto Abn cytogenetic abnormality, ISS International Staging System. Values of Age, CREAT, HGB, and BMPC are given mean  $\pm$  SD.

(Fig. 3A). Excessive ROS suggested that the MM cells were under oxidative stress, which also indicated a possible abnormality in mitochondrial function. Next, we further investigated the mitochondrial membrane potential (MMP) using JC-1 staining. As predicted, we found that after being transfected with PRDX6-siRNA, the MMP declined significantly in both U266 and MM.1S (Fig. 3B). Additionally, oxidative phosphorylation (OXPHOS) is an important process of mitochondrial to produce ATP. To assess the important function of mitochondrial, we examined several OXPHOS genes expression by qRT-PCR, including NADH: ubiquinone oxidoreductase subunit B8, (NDUFB8), succinate dehydrogenase complex iron sulfur subunit B (SDHB), ubiquinol-cytochrome c reductase core protein 2 (UQCRC2) and ATP synthase subunit alpha (ATP5A). As a result, the deficiency of PRDX6 resulted in remarkably decreased expression of OXPHOS genes in both U266 and MM.1S (Fig. 3C).

Based on the above findings that the deficiency of PRDX6 caused significant apoptosis, we wondered about the effect of PRDX6 deficiency on the Bcl-2 family in MM cells. So we detected the expression of the Bax (proapoptotic) and Bcl2 (antiapoptotic) proteins in U266 and MM.1S. The results showed a significant increase in Bax expression and a significant decrease in Bcl2 expression. In addition, western blotting analyses showed more cleavage of PARP and Caspase 3 caused by deficiency of PRDX6, which revealed the consequent activation of the caspase cascade (Fig. 3D). Then the mitochondria ultrastructure was evaluated by transmission electron microscopy (TEM). We found that significant apoptosis and impaired mitochondrial (cristae were markedly decreased and density was increased) in MM.1S when deficiency of PRDX6 (Fig. 3E). The above data showed that excessive ROS and subsequent oxidative stress led to mitochondrial dysfunction, which ultimately

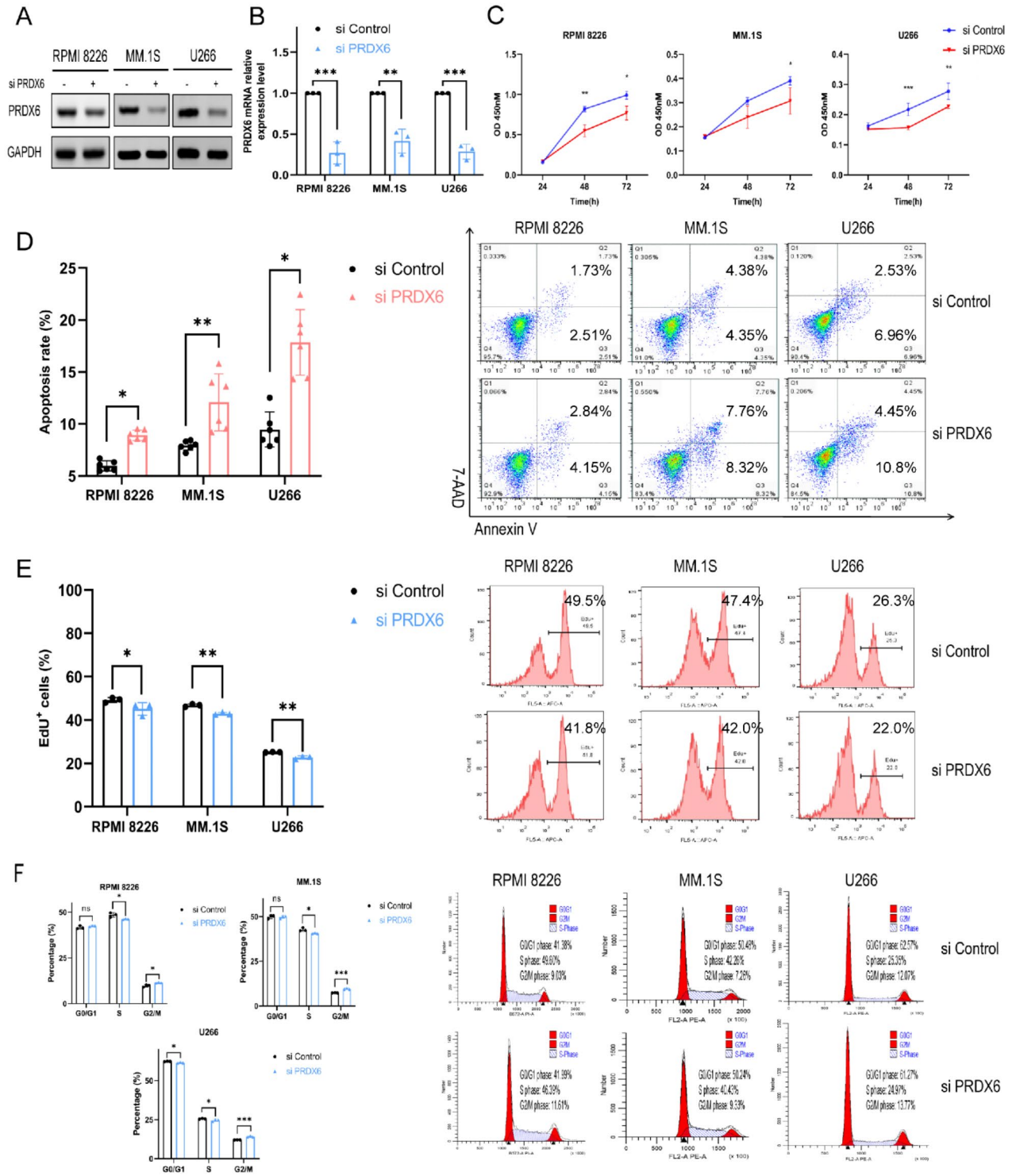


**Fig. 2.** Deficiency of PRDX6 promotes apoptosis and inhibits proliferation in vitro. (A,B) The efficiency of transfection and knock down was assessed by western blotting and qRT-PCR. (C) Cell viability was detected after deficiency using the CCK-8 assay. (D) Cell apoptosis was detected after deficiency using the Annexin V/7-AAD double staining. (E) Cell proliferation was detected after deficiency using the EdU staining. (F) Cell cycle was detected after deficiency using the PI staining. The data are the mean ± SD. \**p* < 0.05, \*\**p* < 0.01, \*\*\**p* < 0.001.



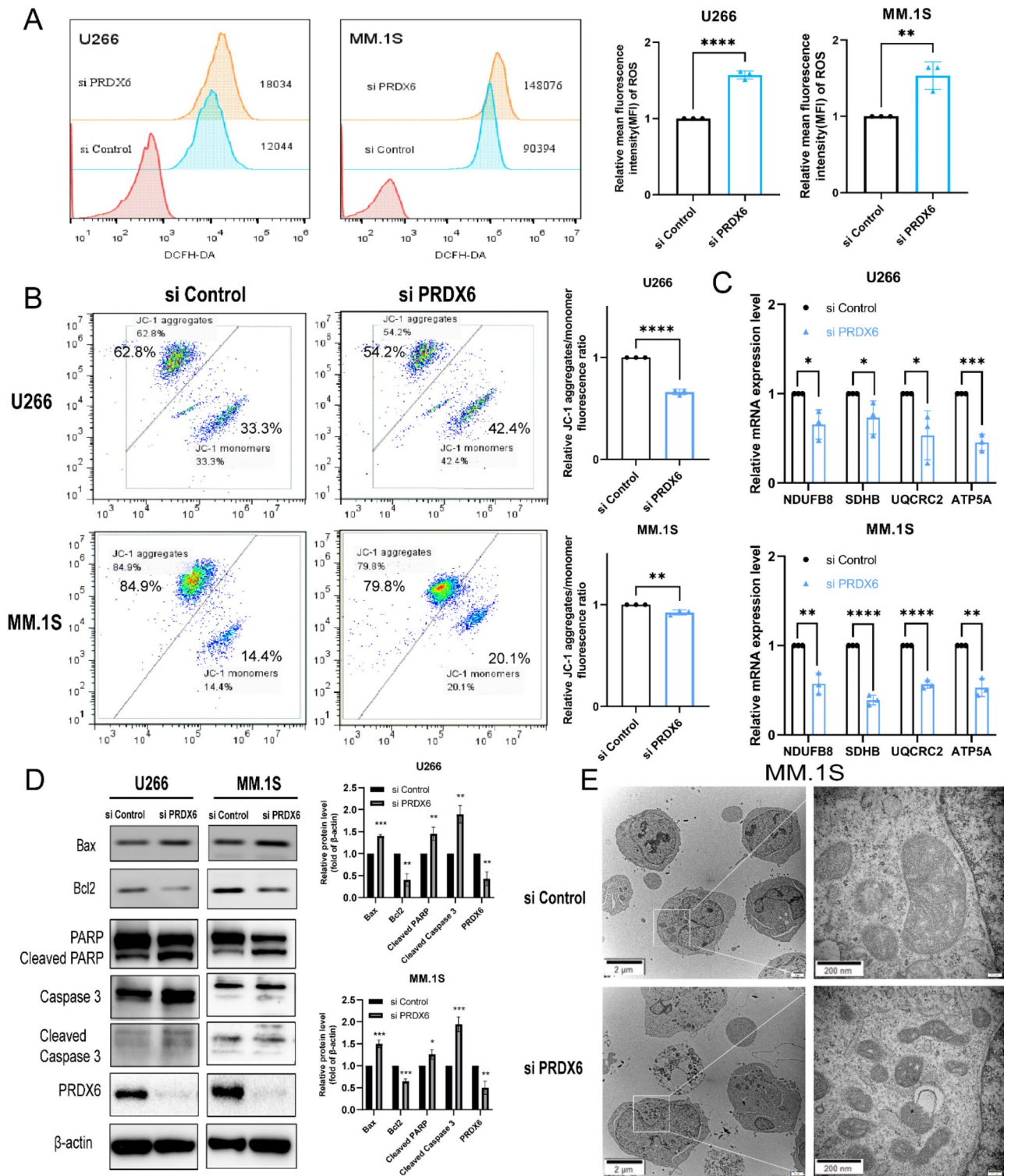


**Fig. 3.** PRDX6 protects MM cells from oxidative stress and maintains mitochondrial homeostasis. **(A)** ROS was detected using 2',7'-dichlorofluorescein diacetate (DCFH-DA) after the deficiency of PRDX6 in U266 and MM.1 S. **(B)** Mitochondrial membrane potential (MMP) was measured using the JC-1 Mitochondrial Membrane Potential Assay Kit following the manufacturer's instructions after the deficiency of PRDX6 in U266 and MM.1 S. **(C)** OXPHOS genes mRNA levels were examined by qRT-PCR in U266 and MM.1 S. **(D)** Bax, Bcl2, PARP, Caspase 3 and their cleaved blots were detected by western blotting using specific antibodies and quantitative analysis was carried out. **(E)** Representative images of mitochondria and cell apoptosis in MM.1S visualized by transmission electron microscopy. The data are the mean  $\pm$  SD. \* $p$  < 0.05, \*\* $p$  < 0.01, \*\*\* $p$  < 0.001, \*\*\*\* $p$  < 0.0001.

caused irreversible cell apoptosis and death. Therefore, PRDX6 is an important antioxidant enzyme, which could eliminate overaccumulation of ROS and maintain the homeostasis of mitochondrial in MM cells.

### Deficiency of PRDX6 improves bortezomib-induced cytotoxicity

As we all know, many drugs have been developed for the treatment of MM, including PIs, immunomodulatory agents, and melphalan. PIs, especially bortezomib, significantly improves MM patients' outcome. Therefore, we wondered whether the anti-tumor activity of bortezomib was altered by combining the deficiency of PRDX6. To our surprise, there was a significant increase in the apoptosis rate after combined treatment (Fig. 4A). This result revealed that the combination treatment was more dramatically effective than single bortezomib treatment in MM cells. Moreover, we also measured the ROS level and MMP to assess the function of mitochondrial after the combined treatment. The results were, the ROS level was further elevated and the MMP was further reduced when combining bortezomib, compared with single bortezomib treatment (Fig. 4B-C). And there was significant cell death and vacuolated mitochondrial in MM.1 S when combined bortezomib with the deficiency of PRDX6 (Fig. 4D). Overall, these data suggested that PRDX6 might be a favorable therapeutic target in MM. It was proved that the administration of bortezomib combined with the deficiency of PRDX6 enhanced cell apoptosis, hence increasing the efficacy of bortezomib alone.

### NAC reverses the effect caused by deficiency of PRDX6

To further confirm whether overaccumulation of ROS and mitochondrial dysfunction were responsible for PRDX6 deficiency-induced apoptosis, a ROS scavenger, N-Acetyl-L-cysteine (NAC) was introduced to pretreat MM cells for 1 h. And then the MM cells were transfected with PRDX6-siRNA to knock down the expression of PRDX6 or treated with bortezomib. As expected, pretreated with NAC partially reversed the PRDX6 deficiency-, bortezomib-, and combined treatment-mediated apoptosis (Fig. 5A), compared with the respective corresponding control group, which was accompanied with elevated MMP in MM.1S (Fig. 5B), and Supplementary Fig. 3 showed the similar results in U266. In addition, we observed that the expression of Bax and Bcl2 were also reversed by NAC, and the cleaved blot of PARP and Caspase 3 were decreased, compared with deficiency group (Fig. 5C). Pretreated with NAC for 1 h, mitochondrial morphology returned normal in MM.1S, compared with deficiency group (Fig. 5D). And the expression of OXPHOS genes were also increased when pretreated with NAC (Fig. 5E). The antioxidant NAC administration blocked uncontrolled ROS overaccumulation, resultant oxidative damage, and mitochondrial dysfunction, suggesting that oxidative stress is responsible for triggering apoptosis and mitochondrial dysfunction by PRDX6 deficiency.

### Deficiency of PRDX6 activates JNK/p38 MAPK signal pathway

It was found that oxidative stress caused by excessive accumulation of ROS could regulate the MAPK signaling pathway. Therefore, we examined the proteins in the MAPK signaling pathway when knocked down PRDX6 and found that the phosphorylation levels of JNK and p38 were elevated, while the total proteins showed no significant changes (Fig. 6A). Subsequently, we introduced p38 inhibitor SB203580 to rescue the effects caused by the deficiency of PRDX6. After PRDX6 deficiency and then treated with SB203580 for 24 h, MM cell apoptosis was detected and the results revealed that cell apoptosis was reduced compared to the knock down group alone (Fig. 6B). Then the MMP was also measured and we found the MMP was increased treated with SB203580, compared to the knock down group alone (Fig. 6C). Moreover, we observed that the expression of Bax and Bcl2 were also reversed by SB203580, and the cleaved blot of PARP and Caspase 3 were decreased, compared with knock down group (Fig. 6D). Finally, we measured the changes in MAPK signaling pathway pretreated with NAC and found that when excess ROS were eliminated with NAC, the phosphorylation levels of JNK and p38 were reduced compared to the knock down group alone (Fig. 6E). All of the above findings suggest that excess ROS can induce oxidative stress in MM cells and mediate the phosphorylation of JNK and p38 in the MAPK signaling pathway, and that the ROS/JNK/p38 MAPK pathway is a potential mechanism for the apoptosis and mitochondrial dysfunction in MM cells induced by PRDX6 deficiency.

### Targeting PRDX6 restrains tumor growth in vivo

To further confirm the role of PRDX6 in vivo, the xenograft tumor animal assay was performed using MM.1 S cells stably transfected with PRDX6-shRNA or control vector (Fig. 7A). The result showed that PRDX6 deficiency had a significant effect on inhibiting tumor growth in vivo, compared with the control group (Fig. 7B,C). Moreover, combination bortezomib and PRDX6 deficiency also had a significant effect on inhibiting tumor growth in vivo, compared with the bortezomib alone (Fig. 7D-F).

H&E staining revealed that the tumor cells in the control group were disorganized, with large deep-stained nuclei, multiple nuclei, and reduced cytoplasm, compared with the knock down group (Fig. 7G). Moreover, the IHC results showed that the proportions of PRDX6-positive, Ki67-positive and Bcl2-positive cells were both decreased in the knock down group, while Cleaved Caspase 3- and Cleaved PARP-positive cells were increased in the knock down group (Fig. 7G). These data indicated that targeting PRDX6 might be a promising strategy to restrain MM progression.

## Discussion

Multiple myeloma (MM) is one of hematological malignancies, characterized by uncontrolled expansion of clonal and aberrant plasma cells in bone marrow. Due to the rapid tumor growth and drugs treatment, MM cells are inevitably susceptible to oxidative stress, which manifested as the inequality between ROS levels and antioxidant defense systems<sup>14</sup>. Oxidative stress has been also implicated in the pathogenesis of solid tumors and degenerative disorders, including Alzheimer's diseases<sup>15</sup>, Parkinson's diseases<sup>16</sup> and cataractogenesis<sup>17</sup>. To cope with the imbalance, tumor cells develop the antioxidant defense systems for their survival and metastasis, which

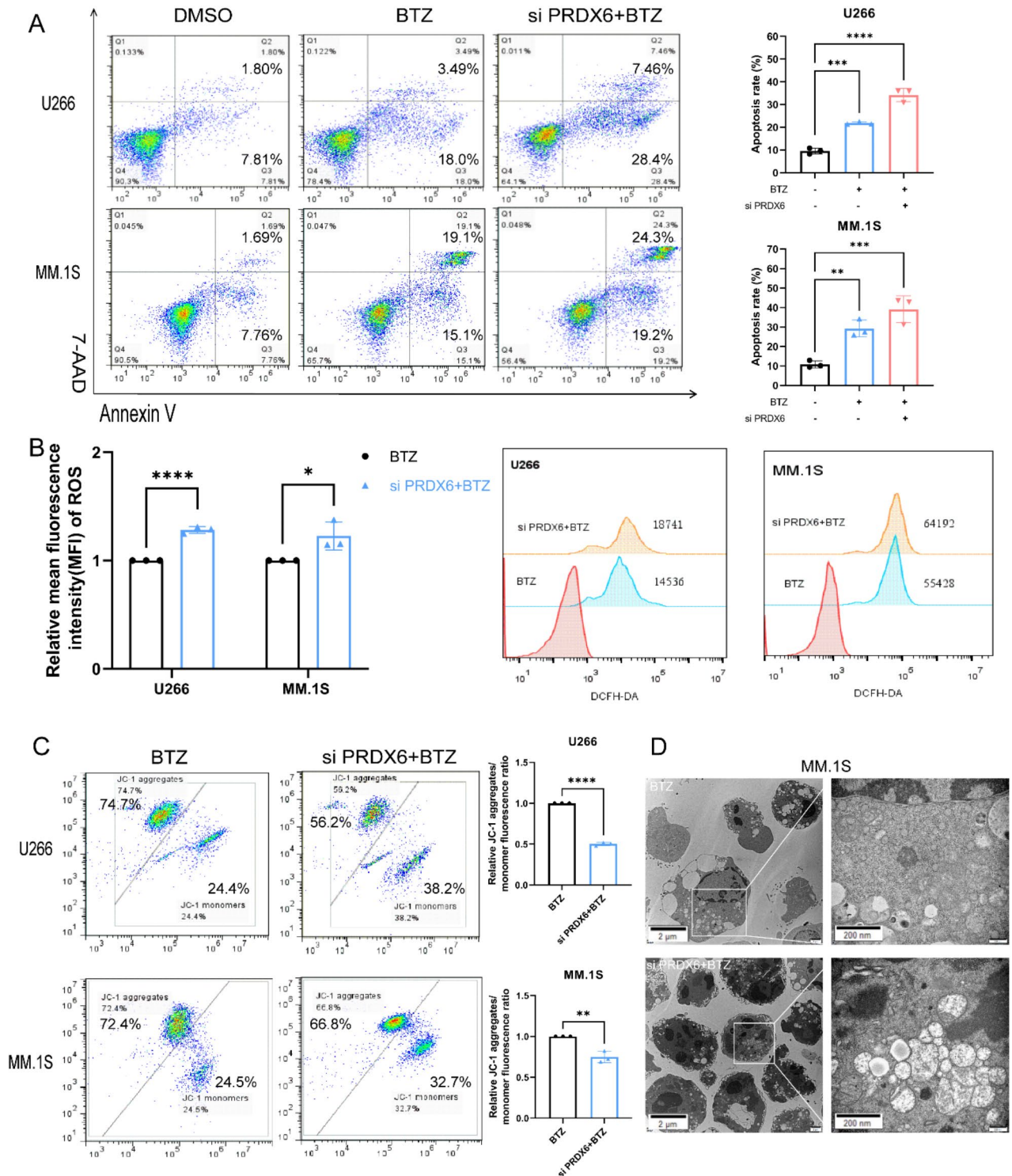


**Fig. 4.** Deficiency of PRDX6 improves bortezomib-induced cytotoxicity. **(A)** Annexin V/7-AAD double staining was used to detect cell apoptosis when combining deficiency with bortezomib (BTZ) in U266 (BTZ = 5nM) and MM.1S (BTZ = 50nM). **(B)** ROS was detected using 2',7'-dichlorofluorescein diacetate (DCFH-DA) when combining deficiency with BTZ in U266 (BTZ = 5nM) and MM.1S (BTZ = 50nM). **(C)** Mitochondrial membrane potential (MMP) was measured using the JC-1 Mitochondrial Membrane Potential Assay Kit following the manufacturer's instructions when combining deficiency with BTZ in U266 (BTZ = 5nM) and MM.1S (BTZ = 50nM). **(D)** Representative images of mitochondria and cell apoptosis in MM.1S visualized by transmission electron microscopy. The data are the mean  $\pm$  SD. \* $p$  < 0.05, \*\* $p$  < 0.01, \*\*\* $p$  < 0.001, \*\*\*\* $p$  < 0.0001.



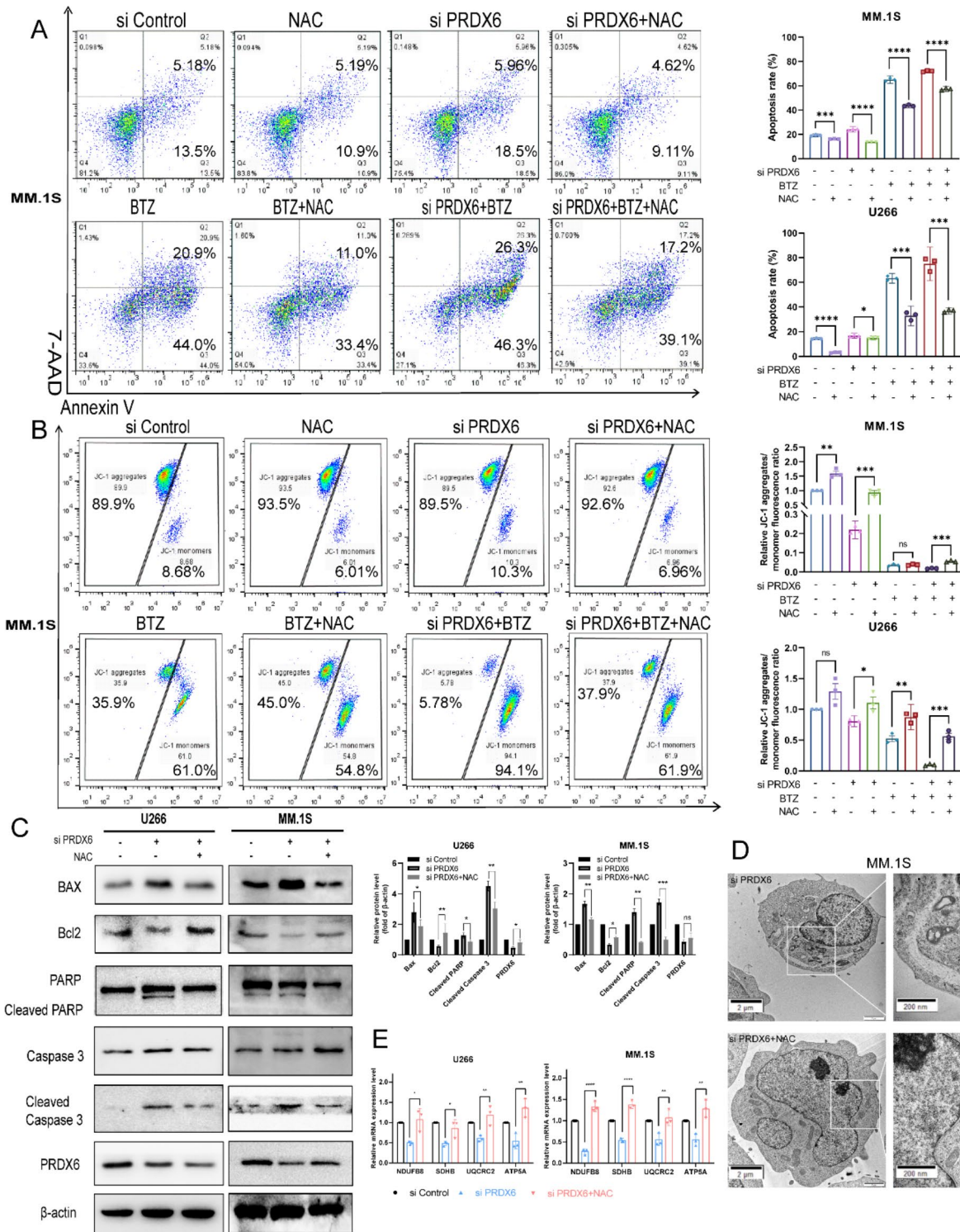


**Fig. 5.** NAC reverses the effect caused by the deficiency of PRDX6. (A–B) After being pretreated with NAC (5 mM) for 1 h, the cells were transfected with PRDX6-siRNA with/without bortezomib in MM.1 S (BTZ = 50nM) and U266 (BTZ = 5nM). Annexin V/7-AAD double staining was used to detect cell apoptosis (A) and JC-1 was used to measure MMP (B). (C) Bax, Bcl2, PARP, Caspase 3 and their cleaved blots were detected by western blotting using specific antibodies and quantitative analysis was carried out. (D) Representative images of mitochondria and cell apoptosis in MM.1S visualized by transmission electron microscopy. (E) OXPHOS genes mRNA levels were examined by qRT-PCR in U266 and MM.1 S. The data are the mean ± SD. \* $p < 0.05$ , \*\* $p < 0.01$ , \*\*\* $p < 0.001$ , \*\*\*\* $p < 0.0001$ , ns: no significance.

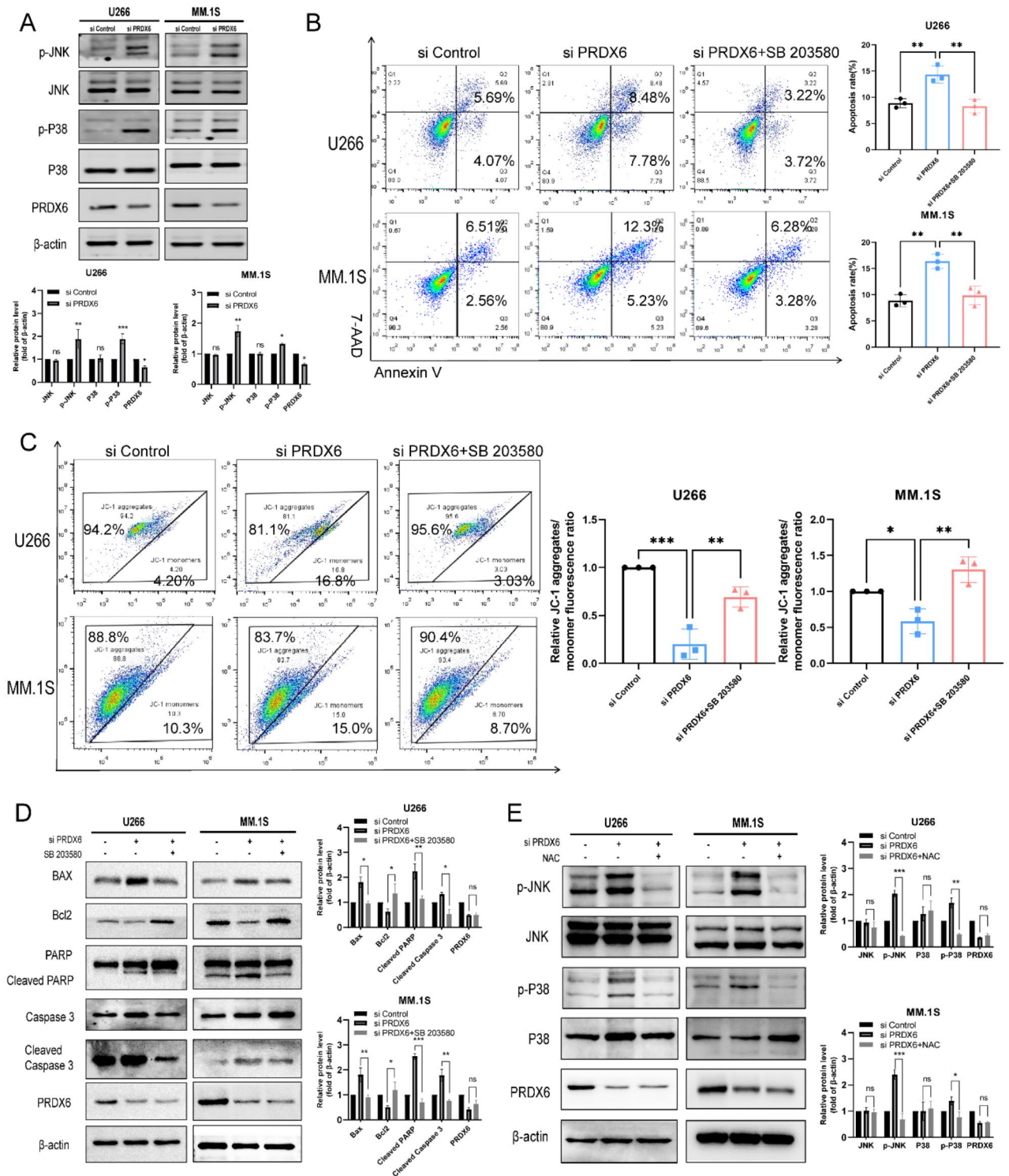


**Fig. 6.** Deficiency of PRDX6 activates JNK/p38 MAPK signal pathway. **(A)** MAPK signal pathway were detected by western blotting using specific antibodies after deficiency of PRDX6 and quantitative analysis was carried out. **(B,C)** After MM cells were transfected with PRDX6-siRNA, then treated with SB203580 (10 mM) for 24 h, Annexin V/7-AAD double staining was used to detect cell apoptosis **(B)** and JC-1 was used to measure MMP **(C)**. **(D)** Bax, Bcl2, PARP, Caspase 3 and their cleaved blots were detected by western blotting using specific antibodies treated with SB203580 (10 mM) for 24 h after deficiency of PRDX6 and quantitative analysis was carried out. **(E)** MAPK signal pathway were detected by western blotting using specific antibodies pretreated with NAC and quantitative analysis was carried out. The data are the mean ± SD. \* $p < 0.05$ , \*\* $p < 0.01$ , \*\*\* $p < 0.001$ , ns: no significance.



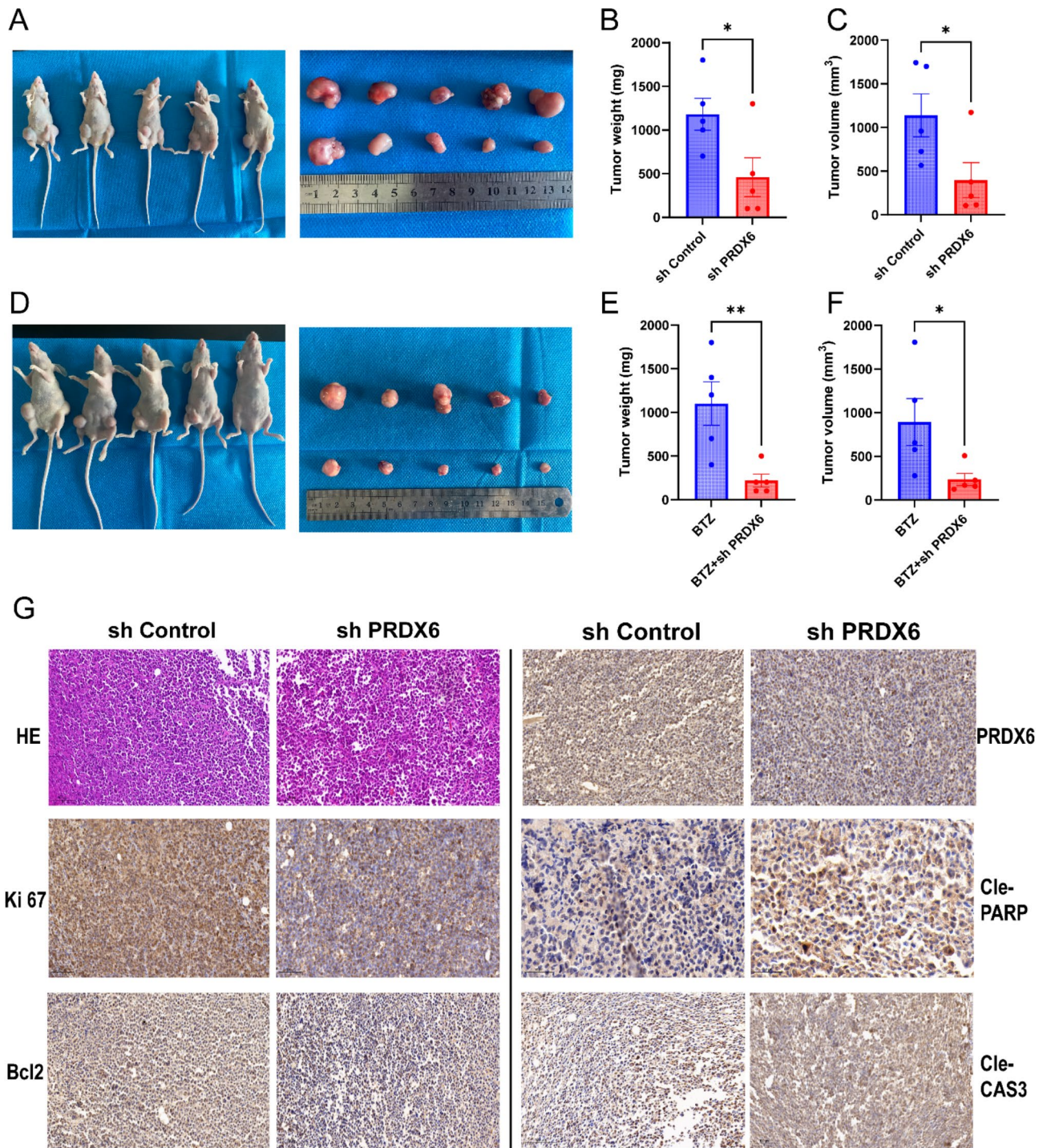


**Fig. 7.** Targeting PRDX6 restrains tumor growth in vivo. (A) Representative images of xenograft tumors from MM tumor-bearing mice in the control and knock down group. (B,C) Tumor weight and volume of xenograft tumors in the control and knock down group. (D) Representative images of xenograft tumors from MM tumor-bearing mice in the BTZ alone and combination group. (E,F) Tumor weight and volume of xenograft tumors in the BTZ alone and combination group. (F) H&E staining and IHC analysis of the protein levels of PRDX6, Ki67, Bcl2, Cleaved Caspase 3 and Cleaved PARP in tumor tissues from the control and deficiency mice bearing MM xenografts. Scale bar, 100  $\mu$ m. The data are the mean  $\pm$  SD. \* $p < 0.05$ , ns: no significance.

include CAT, SODs, GPX, TRX and PRDXs<sup>18</sup>. These proteins could maintain the intracellular redox state and protect tumor cells from cell death under conditions of oxidative stress<sup>19</sup>.

Among them, the PRDXs family is one of the important and highly conserved antioxidant enzymes, which exists in various cellular compartments and can eliminate peroxynitrite, hydrogen peroxide, and organic

hydrogen peroxides<sup>20</sup>. Importantly, PRDX6, the only one 1-Cys PRDX, different from classical glutathione peroxidase or other PRDXs, presents additional activities and involves in various cellular signaling pathways<sup>5</sup>. According to recent studies, the upregulation of PRDX6 is found in many different solid tumors and is associated with migration, invasiveness, chemotherapy resistance, and increasing stem cell properties, especially in NSCLC, colorectal cancer, and esophageal carcinoma<sup>12,21,22</sup>. Targeting the PRDX6 gene has shown that PRDX6 with GSH peroxidase and acidic iPLA2 activity is essential for cell survival, further demonstrating that PRDX6 expression is vital for survival in tumor cells. Fang et al. demonstrated that PRDX6 promoted Toledo DLBCL cell proliferation via peroxidase activity and PRDX6 deficiency induced Toledo DLBCL cell apoptosis<sup>23</sup>. Moreover, PRDX6 might maintain cell integrity by reducing peroxidation of membrane phospholipids, protecting DNA from damage, and controlling survival signalling during oxidative stress<sup>24</sup>.

Although the well-established cytoprotective potential of PRDX6 in solid tumors, there was little information about the role of PRDX6 in MM. Therefore, in our study, we assessed the significance of PRDX6 in MM and we found PRDX6 was upregulated in MM and inversely associated with OS. Furthermore, the deficiency of PRDX6 inhibited cell viability and promoted cell apoptosis via an increased expression of Bax and a decreased expression of Bcl2, accompanied by consequent activation of the caspase cascade (more cleavage of PARP and Caspase 3). The xenograft tumor animal assay also revealed that PRDX6 deficiency inhibited tumor growth. Additionally, bortezomib is the first line of treatment in MM, greatly improving MM patients' outcomes. However, there are many patients who ultimately relapse and become resistant to bortezomib. So, we want to know whether combining PRDX6 deficiency could alter the anti-tumor effect of bortezomib in MM cells. Intriguingly, we noted that the combined treatment induced more apoptotic cells and intense oxidative stress than did bortezomib alone. These data provide novel insight that PRDX6 may be a target for enhancing the efficacy of bortezomib for MM patients.

Mechanically, previous studies reported that PRDX6 could positively regulate oncogenesis and progression by activating the JAK2/STAT3 signalling pathway. Moreover, PRDX6 regulates Erk1/2 phosphorylation, and Erk1/2 activation also promotes PRDX6 gene expression, finally resulting in a positive feedback loop<sup>25,26</sup>. Given that PRDX6 is an antioxidant, we measured intracellular ROS levels, which elevated obviously after the deficiency of PRDX6. These data revealed that PRDX6 deficiency led to over-accumulation of ROS in MM cells. ROS was thought to be the by-product of normal metabolism<sup>27</sup> but was elevated largely when faced with oxidative stress, including hydrogen peroxide (H<sub>2</sub>O<sub>2</sub>), hydroxyl radical ( $\cdot$ OH), superoxide radical ( $\cdot$ O<sub>2</sub><sup>-</sup>), and oxygen (O<sub>2</sub>). It has been indicated that ROS is an important regulatory factor related to a series of biological phenomena, especially in tumors<sup>28</sup>. Some research has shown that ROS is a common mediator to promote apoptosis. The high level of ROS is deleterious, due to subsequent oxidative stress induces cell apoptosis or necrosis. Thus, intracellular ROS generation and elimination are tightly regulated in tumor cells. In our study, the deficiency of PRDX6 resulted in ROS accumulation and initiated oxidative stress, thus triggering MM cells apoptosis.

MAPK (Mitogen activated protein kinase) is involved in the regulation of cell proliferation, differentiation, transformation, and apoptosis through the phosphorylation of nuclear transcription factors, cytoskeletal proteins, and enzymes, and is closely related to inflammation, tumors, and other diseases. The MAPK signaling pathway includes four protein kinases, including ERK, JNK/SAPK, p38 MAPK, and ERK5/BMK1. The MAPK signaling pathway has been found to play an important role in the regulation of oxidative stress, inflammation, calcium overload, etc<sup>29</sup>. The MAPK cascade kinase can be activated continuously in response to intracellular ROS accumulation and oxidative stress, mediate the activation of apoptosis initiator Caspase 9 and apoptosis executioner Caspase 3, and regulate the expression of the Bcl-2 family of proteins, which are involved in the regulation of the apoptotic cell death process. The Bcl-2 family of proteins is regulated, thus participating in the regulation of apoptotic cell death. In our study, we also found that excess ROS can mediate the phosphorylation of JNK and p38 in the MAPK signaling pathway, following the imbalance in the expression of Bax and Bcl2, then the cleavage of PARP and Caspase 3 increased. Therefore, the ROS/JNK/p38 MAPK pathway is a potential mechanism for the apoptosis and mitochondrial dysfunction in MM cells induced by PRDX6 deficiency.

Additionally, excess oxidative stress which broke the balance of redox homeostasis could lead to irreversible damage to cells, such as protein damage, mitochondrial dysfunction<sup>30</sup>, a wide range of DNA lesions, and even genomic instability<sup>31</sup>. Mitochondria is an indispensable component in tumor cells, which is essential to tumorigenesis, apoptosis, cancer therapy, and metastasis by orchestrating cellular energy production or transformation and ROS signalling pathway. Studies have reported a tight relationship between PRDX6 and mitochondrial dysfunction, and mitophagy was significantly increased in HepG2 cells after PRDX6 knockout<sup>31</sup>. Phosphorylation of PRDX6 can be targeted to acidic organelles and translocate to damaged mitochondrial membranes<sup>32</sup>. Consistently, our study found the MMP was decreased after the deficiency of PRDX6 in MM cells. Increased JC-1 monomers represented depolarized or inactive mitochondria, which showed up decreased membrane potential and could not effectively eliminate ROS. The depolarized MMP feed-forward promoting ROS production resulted in more serious damage. As an important function of the mitochondrial, OXPHOS is particularly important in the process of producing ATP. To assess this important function of mitochondrial, we checked several OXPHOS genes expression. Deficiency of PRDX6 resulted in remarkably decreased expression of OXPHOS genes, but the specific regulatory mechanism remains to be explored in future work.

Collectively, the deficiency of PRDX6 led to ROS overaccumulation and oxidative stress in MM cells, which resulted in activation of MAPK signal pathway, ultimately mitochondrial dysfunction by decreasing MMP, disturbing the mitochondrial respiration process, and generating more damaged mitochondria. Subsequently, the dysfunctional mitochondria produced more ROS, which eventually aggravated mitochondrial dysfunction. And its deficiency could increase the susceptibility of cells to bortezomib and induce robust apoptosis in MM cells (Fig. 8). Hence, PRDX6 is a crucial enzyme for anti-oxidative response and should be a meaningful biomarker and potential therapeutic target in MM patients. However, there are still some shortcomings, (i)



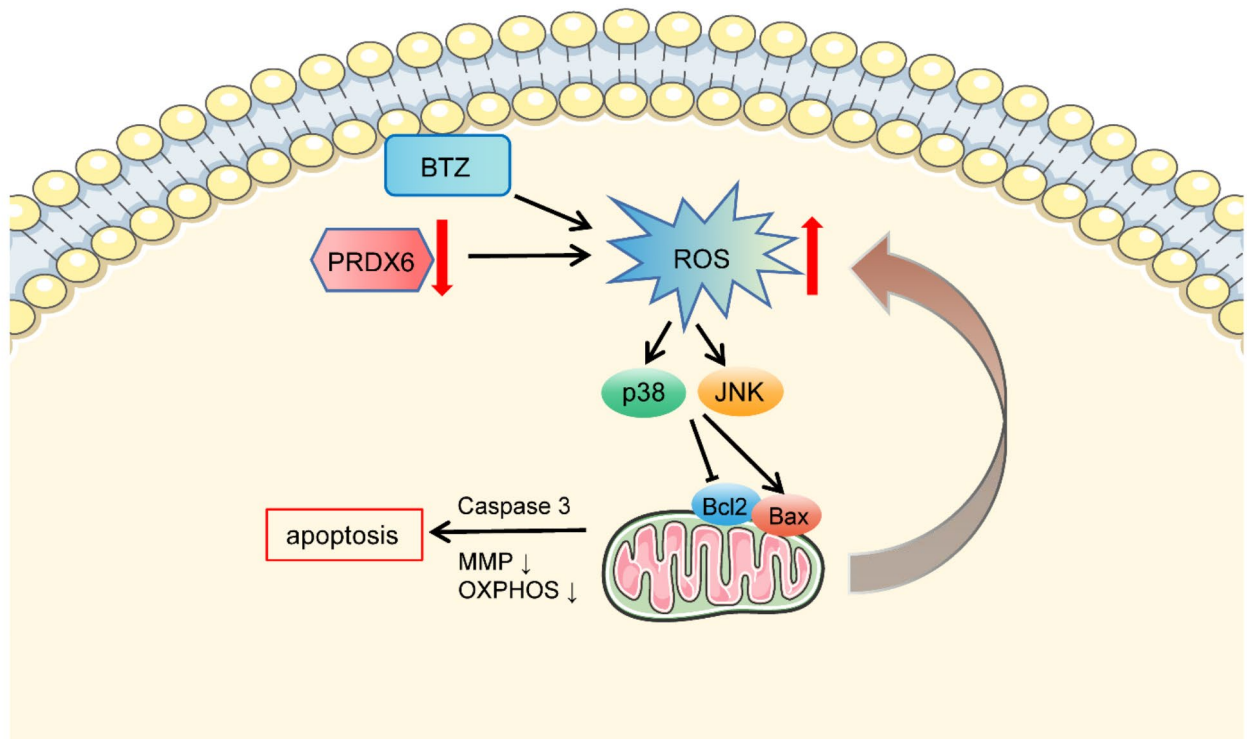


**Fig. 8.** The graphic working model illustrated that PRDX6 deficiency promotes cell apoptosis through overaccumulation of ROS, activation of MAPK signal pathway, decreased MMP, and mitochondrial dysfunction. And PRDX6 deficiency enhanced bortezomib-induced cytotoxicity in MM.

the clinical bone marrow sample sizes of NDMM are too small to properly represent the general facts; (ii) the underlying and complicated mechanism needs to be further explored.

## Materials and methods

### Cell lines and cell culture

The human multiple myeloma cell lines (U266, MM.1S, RPMI 8226, NCI-H929, OPM2, HS5) were obtained from professor Jinsong Hu of Xi'an Jiaotong University. All these cell lines were identified by STR (Short Tandem Repeat) before the experiments were carried out. Cell lines were grown in RPMI1640 medium (BasalMedium, China) replenished with 10% fetal bovine serum (FBS, Biological Industries, Israel), 100 µg/ml L-glutamine and antibiotics, and incubated in humidified air with 5% CO<sub>2</sub> atmosphere at 37°C.

### Materials and reagents

The antibodies including rabbit anti-GAPDH (#10494, 1:1000), rabbit anti-PRDX6 (#13585, 1:1000), rabbit anti-Bax (#50599, 1:3000), rabbit anti-Bcl2 (#12789, 1:1000), mouse anti-PARP (#66520, 1:1000), rabbit anti-Caspase 3 (#19677, 1:1000), rabbit anti-JNK (#17572, 1:1000), rabbit anti-p38 (#51115, 1:1000), rabbit anti-Phospho-p38 (#28796, 1:1000) and mouse anti-β-actin (#66009, 1:1000) were bought from Proteintech (USA). Rabbit anti-Phospho-JNK (#4668, 1:1000) was bought from CST (USA). Bortezomib (HY-10227) and p38 MAPK inhibitor SB203580 (HY-10256) were purchased from MedChemExpress (Shanghai, China). N-Acetyl-L-cysteine (A9165) was obtained from Sigma (Sigma-Aldrich, St Louis, MO, USA) and diluted to 5 mM as the final concentration. Puromycin (CAS:58-58-2) was from Solarbio (China).

### Cell viability

Cell viability was checked by the Cell Counting Kit-8 assay (CCK-8, 7 sea, Shanghai, China). Cells at the logarithmic growth phase were seeded in 96-well plates at a density of  $2 \times 10^4$  cells per well for the indicated times. After transfection with PRDX6-siRNA for 24, 48 and 72 h, 10 µl of CCK8 solution was added to each well and the plates continued incubating for 1–4 h at 37°C. Then, Thermo Scientific™ Multiskan™ FC was used to detect the OD values at a wavelength of 450 nm.

### Cell apoptosis, cell proliferation, and cell cycle

To measure cell apoptosis, proliferation, and cell cycle, flow cytometry was carried out. Briefly,  $1 \times 10^6$  cells per well were seeded in 6-well plates, then exposed to indicated concentrations of bortezomib with/without deficiency of PRDX6 for 24/48 hours. The cell samples were harvested, then stained with 5 µl of 7-amino-actinomycin D (7-AAD, BD Biosciences, San Jose, CA, USA) and 5 µl of Annexin V-fluorescein isothiocyanate (FITC, BD Biosciences) in 50 µl of binding buffer and incubated at 4°C for 15 min. Then, the binding buffer was

applied and immediately recorded using a FACS Canto II flow cytometer (BD Biosciences); 10,000 events were recorded and analyzed.

Cell cycle was measured by PI staining. Cell samples were fixed with 70% ethanol overnight at 4 °C. Then, the cells were incubated with RNase A and PI per the manufacturers' protocol (Beyotime, China). DNA content was then analyzed using a FACS Canto II flow cytometer; 30,000 events were recorded and analyzed.

Cell proliferation was measured by EdU assay. Cell samples were fixed with EdU(1x) at 37 °C for 2 h. Then, the cells were harvested, fixed for 15 min, permeable for 15 min as the manufacturers' protocol (Beyotime, China). EdU positive cells were then analyzed using a FACS Canto II flow cytometer; 10,000 events were recorded and analyzed. FlowJo 7.6.2 software was used to analyze these data.

### MM patients and healthy donors

All patients and healthy donors provided written informed consent of using their samples for research purposes. BM aspirates were obtained from patients newly diagnosed with MM and healthy donors. Ficoll-Hipaque density sedimentation was used to isolate mononuclear cells. The study was approved by the ethical committee of Xi'an Jiaotong University (2015 – 186) and performed following relevant named guidelines and regulations. The study was carried out in compliance with the ARRIVE guidelines.

### Bioinformatic analysis

Gene expression profiles of GSE6477 ( $n = 162$ ), GSE47552 ( $n = 99$ ) and GSE13591 ( $n = 158$ ) were derived from GEO (<https://www.ncbi.nlm.nih.gov/geo/>). GEO2R was carried out to analyze the mRNA expression in BM of healthy donors or different stages of plasma cell neoplasm. ROC curve was evaluated based on gene expression in GSE6477. Survival curves were created using the Kaplan-Meier method in patients of GSE24080 ( $n = 559$ ) and GSE57317 ( $n = 55$ ), and any differences in the survival curves were compared by the log-rank test.

### Transfection of small interfering RNA (siRNA) and short hairpin RNA (shRNA)

MM cells were transiently transfected with siRNA (GenePharma, Shanghai, China) targeting a negative control or PRDX6 at a final concentration of 100 nM using Rfect siRNA/miRNA Transfection Reagent (Baidai biotechnology, China) according to manufacturer's instructions. The sequences for siRNA of human PRDX6 and negative control was in Supplementary Table 1.

Lentiviral vector containing human PRDX6 shRNA were purchased from Genepharma (Shanghai, China), which was used to deficiency PRDX6 in MM.1 S cells. After 48 h, transfected cells were treated with 2.5 µg/ml puromycin, then the cells were harvested for further animal experimentation.

### Transmission electron microscopy

Cells were collected by centrifugation and fixed in 2.5% glutaraldehyde in 0.1 mol/L phosphate buffer (pH 7.4) for 30 min, post fixed in 1% osmium tetroxide in the same buffer for 30 min, dehydrated in graded ethanol, washed with propylene oxide, embedded in Epon, and then sectioned on an ultramicrotome at 90 nm thickness. Thin sections were stained with 5% uranyl acetate and 5% lead citrate and then examined on a HITACHI (H-7650) transmission electron microscope at 80 kV.

### Assessment of mitochondrial membrane potential (MMP)

The cells underwent the same processing described in 2.4., 24–48 h after transfection of PRDX6-siRNA with/without bortezomib, the MMP of cells was evaluated using JC-1 staining (Beyotime, China) following the manufacturer's protocol. By using flow cytometry, we determined 488 nm for JC-1 monomers and 525 nm for JC-1 aggregates, respectively. MMP was measured to compare the ratio of JC-1 monomers/JC-1 aggregates.

### Determination of intracellular reactive oxygen species (ROS)

2',7'-dichlorofluorescein diacetate (DCFH-DA, Beyotime, China) staining was used to detect intracellular ROS levels. After transfection of PRDX6-siRNA with/without bortezomib, the cells were harvested and incubated with DCFH-DA (10 µM) for 20 min at 37 °C in the dark, then the ROS levels were measured using flow cytometry.

### Quantitative real-time polymerase chain reaction (qRT-PCR)

Total RNA was extracted from treated MM cells using TRIzol reagent (CWBI, China). RNA concentrations were measured by Nanodrop and reverse-transcribed to cDNA using the cDNA Reverse Transcription Kit (CWBI, China). qRT-PCR was performed using the SYBR Green PCR kit (CWBI, China) and the three-step method was applied. Pre-denatured at 95 °C for 5 min, denatured at 95 °C for 10 s, annealed at 55–60 °C for 20 s, and extended at 72 °C for 20 s, the last three steps require 40 cycles. The primers are listed. GAPDH was used as control. The  $2^{-\Delta Ct}$  or  $2^{-\Delta\Delta Ct}$  method were used for analysis. The primers were showed in Supplementary Table 2.

### Western blotting

Cells were lysed in lysis buffer and loaded on 12.5% SDS-PAGE gel with equal amounts of proteins, then electro-transferred to PVDF membrane. After blocking for 1.5 h in 5% non-fat dry milk in PBS with Tween 20 (PBST) buffer and incubated with specific primary antibodies overnight at 4 °C. After washing with PBST three times, the appropriate secondary antibodies were added. Then incubated at room temperature for 1 h and visualized using the ECL Western Blot Detection kit (Biosharp, China). The pictures were captured with a CCD camera system (MiniChem610) and analyzed by Image J.

### Xenograft tumor mice model

Female BALB/c-Nude mice (3–4 weeks, Gempharmatech, China) were obtained and kept in SPF environment. The mice were randomly divided into control group ( $n = 5$ ) and knock down group ( $n = 5$ ). For subcutaneous xenotransplanted tumor model, 100  $\mu$ l serum-free RPMI1640 medium containing Matrigel (Corning) (1:1, v/v) and  $5 \times 10^6$  cells per well were seeded in 6-well plates cells were injected subcutaneously into flanks of the mice. Then  $5 \times 10^6$  cells per well were seeded in 6-well plates MM.1 S cells with PRDX6 deficiency were subcutaneously injected per mouse in knock down group. And  $5 \times 10^6$  MM.1 S cells with lentivirus-NC were subcutaneously injected per mouse in control group. About 24 days after tumor cell injection, the mice were sacrificed and xenograft tumors were harvested, weighed and processed for immunohistochemistry staining. At the same time, the changes in body weight of mice were recorded every four days. Tumor volume ( $V = a \times b^2 / 2$ ; a: the largest superficial diameter, b: the smallest superficial diameter). The study was approved by the ethical committee of Xi'an Jiaotong University (2022 – 1494) and performed following relevant named guidelines and regulations. The study was carried out in compliance with the ARRIVE guidelines.

### Immunohistochemistry (IHC) and histological analysis

Paraffin-embedded thin sections (4  $\mu$ m) of tumor tissues were deparaffinized, rehydrated, antigen retrieved, and incubated with primary antibodies overnight at 4 °C. Following incubated with secondary antibodies, sections were treated with DAB and hematoxylin prior to visualized with a light microscope (Nikon, Tokyo, Japan). The tumor tissues of mice were also stained with hematoxylin & eosin (H&E) to assess the morphology of tumor cells.

### Statistical analysis

Statistical analysis was analyzed by unpaired Student's t-test between two experimental groups. One-way ANOVA was used to compare multiple groups through S-N-K or Dunnett's T3 test and Mann-Whitney U test. Data are presented as mean  $\pm$  SD as indicated by at least three independent experiments. The GraphPad Prism 9 Software (La Jolla, CA, USA) was used to analyze data.  $P < 0.05$  was considered statistically significant.

### Data availability

Data is provided within the manuscript or supplementary information files.

Received: 13 March 2024; Accepted: 19 December 2024

Published online: 02 January 2025

### References

- Chim, C. S. et al. Management of relapsed and refractory multiple myeloma: novel agents, antibodies, immunotherapies and beyond. *Leukemia* **32**(2), 252–262. <https://doi.org/10.1038/leu.2017.329> (2017).
- Gandolfi, S. et al. The proteasome and proteasome inhibitors in multiple myeloma. *Cancer Metastasis Rev.* **36**(4), 561–584. <https://doi.org/10.1007/s10555-017-9707-8> (2017).
- Robak, P., Drozd, L., Szemraj, J. & Robak, T. Drug resistance in multiple myeloma. *Cancer Treat. Rev.* **70**, 199–208. <https://doi.org/10.1016/j.ctrv.2018.09.001> (2018).
- Rhee, S. G., Woo, H. A., Kil, I. S. & Bae, S. H. Peroxiredoxin functions as a peroxidase and a regulator and sensor of local peroxides. *J. Biol. Chem.* **287**(7), 4403–4410. <https://doi.org/10.1074/jbc.r111.283432> (2012).
- Arevalo, J. & Vázquez-Medina, J. The role of peroxiredoxin 6 in cell signaling. *Antioxidants* **7**(12), 172. <https://doi.org/10.3390/antiox7120172> (2018).
- Zhou, S. et al. Functional interaction of glutathione S-transferase pi and peroxiredoxin 6 in intact cells. *Int. J. Biochem. Cell Biol.* **45**(2), 401–407. <https://doi.org/10.1016/j.biocel.2012.11.005> (2013).
- Fisher, A. B. et al. A novel lysophosphatidylcholine acyl transferase activity is expressed by peroxiredoxin 6. *J. Lipid Res.* **57**(4), 587–596. <https://doi.org/10.1194/jlr.m064758> (2016).
- Yun, H-M. et al. PRDX6 promotes lung tumor progression via its GPX and iPLA2 activities. *Free Radic. Biol. Med.* **69**, 367–376. <https://doi.org/10.1016/j.freeradbiomed.2014.02.001> (2014).
- Huang, C-F. et al. Increased expression of peroxiredoxin 6 and cyclophilin A in squamous cell carcinoma of the tongue. *Oral Dis.* **17**(3), 328–334. <https://doi.org/10.1111/j.1601-0825.2010.01730.x> (2010).
- Pak, J. H. et al. Peroxiredoxin 6 overexpression attenuates Cisplatin-Induced apoptosis in human ovarian Cancer cells. *Cancer Invest.* **29**(1), 21–28. <https://doi.org/10.3109/07357907.2010.535056> (2010).
- Pagaza-Straffon, C. et al. Evaluation of a panel of tumor-associated antigens in breast cancer. *Cancer Biomarkers.* **27**(2), 207–211. <https://doi.org/10.3233/cbm-190708> (2020).
- Xu, J. et al. Differential expression and effects of peroxiredoxin-6 on drug resistance and cancer stem cell-like properties in non-small cell lung cancer. *Oncotargets Ther.* **12**, 10477–10486. <https://doi.org/10.2147/ott.s211125> (2019).
- Sahu, N. et al. Functional screening implicates mir-371-3p and peroxiredoxin 6 in reversible tolerance to cancer drugs. *Nat. Commun.* **7**(1). <https://doi.org/10.1038/ncomms12351> (2016).
- Caillet, M., Dakik, H., Mazurier, F. & Sola, B. Targeting reactive oxygen species metabolism to induce myeloma cell death. *Cancers (Basel)* **13**(10), 2411. <https://doi.org/10.3390/cancers13102411> (2021).
- Panahzadeh, F., Mirnasuri, R. & Rahmati, M. Exercise and Syzygium aromaticum reverse memory deficits, apoptosis and mitochondrial dysfunction of the hippocampus in Alzheimer's disease. *J. Ethnopharmacol.* **286**, 114871. <https://doi.org/10.1016/j.jep.2021.114871> (2022).
- Mohammadipour, A. A focus on natural products for preventing and cure of mitochondrial dysfunction in Parkinson's disease. *Metab. Brain Dis.* <https://doi.org/10.1007/s11011-022-00931-8> (2022).
- Quan, Y. Connexin gap junctions and hemichannels in modulating lens redox homeostasis and oxidative stress in cataractogenesis. *Antioxidants (Basel)* **10**(9), 1374 (2021).
- Rhee, S. G., Chae, H. Z. & Kim, K. Peroxiredoxins. A historical overview and speculative preview of novel mechanisms and emerging concepts in cell signaling. *Free Radic. Biol. Med.* **38**(12), 1543–1552. <https://doi.org/10.1016/j.freeradbiomed.2005.02.026> (2005).
- Bannitz-Fernandes, R. et al. Non-mammalian Prdx6 enzymes (proteins with 1-Cys prdx mechanism) Display PLA2 activity similar to the human orthologue. *Antioxidants* **8**(3), 52. <https://doi.org/10.3390/antiox8030052> (2019).

20. Fatma, N. et al. Peroxiredoxin 6 delivery attenuates TNF- $\alpha$ - and glutamate-induced retinal ganglion cell death by limiting ROS levels and maintaining Ca<sup>2+</sup> homeostasis. *Brain Res.* **1233**, 63–78. <https://doi.org/10.1016/j.brainres.2008.07.076> (2008).
21. Huang, W.-S. Expression of PRDX6 correlates with migration and invasiveness of colorectal cancer cells. *Cell. Physiol. Biochem. Published Online.* <https://doi.org/10.1159/000495934> (2018).
22. He, Y. et al. Overexpression of peroxiredoxin 6 (PRDX6) promotes the aggressive phenotypes of esophageal squamous cell carcinoma. *J. Cancer.* **9**(21), 3939–3949. <https://doi.org/10.7150/jca.26041> (2018).
23. Fang, Z. et al. PRDX6 promotes proliferation and induces chemo-resistance via peroxidase activity in Toledo diffuse large B-cell lymphoma cells. *Transl Cancer Res.* **8**(5), 1772–1781. <https://doi.org/10.21037/tcr.2019.08.36> (2019).
24. Manevich, Y. et al. Binding of peroxiredoxin 6 to substrate determines differential phospholipid hydroperoxide peroxidase and phospholipase A2 activities. *Arch. Biochem. Biophys.* **485**(2), 139–149. <https://doi.org/10.1016/j.abb.2009.02.008> (2009).
25. Yun, H.-M. et al. PRDX6 promotes tumor development via the JAK2/STAT3 pathway in a urethane-induced lung tumor model. *Free Radic. Biol. Med.* **80**, 136–144. <https://doi.org/10.1016/j.freeradbiomed.2014.12.022> (2015).
26. Zha, X. et al. PRDX6 protects ARPE-19 cells from oxidative damage via PI3K/AKT signaling. *Cell. Physiol. Biochem.* **36**(6), 2217–2228. <https://doi.org/10.1159/000430186> (2015).
27. Reczek, C. R. & Chandel, N. S. ROS-dependent signal transduction. *Curr. Opin. Cell Biol.* **33**, 8–13. <https://doi.org/10.1016/j.ccb.2014.09.010> (2015).
28. Holmström, K. M. & Finkel, T. Cellular mechanisms and physiological consequences of redox-dependent signalling. *Nat. Rev. Mol. Cell Biol.* **15**(6), 411–421. <https://doi.org/10.1038/nrm3801> (2014).
29. Sorokina, E. M. et al. Intracellular targeting of peroxiredoxin 6 to lysosomal organelles requires MAPK activity and binding to 14-3-3 $\epsilon$ . *Am. J. Physiol. Cell. Physiol.* **300**(6), C1430–C1441 (2011).
30. Basel-Vanagaite, L. et al. Deficiency for the ubiquitin ligase UBE3B in a blepharophimosis-ptosis-intellectual-disability syndrome. *Am. J. Hum. Genet.* **91**(6), 998–1010. <https://doi.org/10.1016/j.ajhg.2012.10.011> (2012).
31. Kim, T. H. et al. Piperlongumine treatment inactivates peroxiredoxin 4, exacerbates endoplasmic reticulum stress, and preferentially kills high-grade glioma cells. *Neuro-Oncology* **16**(10), 1354–1364. <https://doi.org/10.1093/neuonc/nou088> (2014).
32. López-Grueso, M. J. et al. Knockout of PRDX6 induces mitochondrial dysfunction and cell cycle arrest at G2/M in HepG2 hepatocarcinoma cells. *Redox Biol.* **37**, 101737. <https://doi.org/10.1016/j.redox.2020.101737> (2020).

## Acknowledgements

We sincerely thank you for the help provided by all lab personnel in this research.

## Author contributions

D.G.: Conceptualization, Investigation, Methodology, Software, Validation, Data curation, Formal analysis, Writing—original draft, Visualization. Y.L.: Methodology, Validation, Data curation, Formal analysis, Investigation, Visualization. F.H.: Methodology, Investigation, Visualization. D.W.: Software, Validation. T.W.: Specimen collection. G.G.: Methodology, Investigation, Visualization. Z.L.: Conceptualization, Validation. R.Y.: Conceptualization, Validation. J.H.: Methodology. A.H.: Supervision, Writing—review & editing. P.Z.: Supervision, Writing—review & editing. All authors reviewed the manuscript.

## Funding

This work was supported by Natural Science Foundation of Shaanxi Province (Grant Number No. 2022JQ-812).

## Declarations

## Competing interests

The authors declare no competing interests.

## Additional information

**Supplementary Information** The online version contains supplementary material available at <https://doi.org/10.1038/s41598-024-84021-y>.

**Correspondence** and requests for materials should be addressed to A.H. or P.Z.

**Reprints and permissions information** is available at [www.nature.com/reprints](http://www.nature.com/reprints).

**Publisher's note** Springer Nature remains neutral with regard to jurisdictional claims in published maps and institutional affiliations.

**Open Access** This article is licensed under a Creative Commons Attribution-NonCommercial-NoDerivatives 4.0 International License, which permits any non-commercial use, sharing, distribution and reproduction in any medium or format, as long as you give appropriate credit to the original author(s) and the source, provide a link to the Creative Commons licence, and indicate if you modified the licensed material. You do not have permission under this licence to share adapted material derived from this article or parts of it. The images or other third party material in this article are included in the article's Creative Commons licence, unless indicated otherwise in a credit line to the material. If material is not included in the article's Creative Commons licence and your intended use is not permitted by statutory regulation or exceeds the permitted use, you will need to obtain permission directly from the copyright holder. To view a copy of this licence, visit <http://creativecommons.org/licenses/by-nc-nd/4.0/>.

© The Author(s) 2024